# Electrically modulated Josephson junction of light-dressed topological insulators

Pei-Hao Fu [1,2] Yong Xu,[1,2] Xiang-Long Yu,[3,4] Jun-Feng Liu [5,*] and Jiansheng Wu[2,3,4,†]

[1]*Department of Physics, Harbin Institute of Technology, Harbin 150001, China*
[2]*Department of Physics, Southern University of Science and Technology, Shenzhen 518055, China*
[3]*Shenzhen Institute for Quantum Science and Engineering (SIQSE), Southern University of Science and Technology, Shenzhen, China*
[4]*International Quantum Academy (SIQA), Shenzhen 518055, China*
[5]*School of Physics and Materials Science, Guangzhou University, Guangzhou 510006, China*

In a Josephson junction mediated by a two-dimensional irradiated topological insulator, the current-phase relation can be electrically modulated, including the 0-$\pi$ phase transition and the anomalous phase shift of the current. Qualitatively combining analyses and numerical simulations, we find that the 0-$\pi$ phase transition and anomalous phase shift can be controlled by a gate voltage and a transverse electric field, respectively. These possible electrical modulations result from the photoinduced anisotropic helical edge states. Due to the anisotropy and spin-momentum locking nature in the edge channels, an effective Zeeman field is caused by an electrical potential whose orientation automatically matches the spin alignment of the edge modes. The photoinduced anisotropy provides potential applications in Flouqet engineering helical supercurrent and electrically modulated topological superconducting devices.

## I. INTRODUCTION

In two dimensions, topological insulators (TIs) or quantum spin Hall insulators (QSHIs), characterized by helical edge states that are topologically protected by the insulating bulk state have aroused intense researching interest [1,2]. Guaranteed by time reversal symmetry, the helical edge states are isotropic, i.e., the velocities of edge modes are of the same magnitude, but with directions of motion locked to the value of the spin projection [3–5]. The helical edge states are experimentally observed in HgTe/CdTe quantum wells [6–9], InAs/GaSb quantum wells [10,11], and WTe$_2$ monolayers [12,13]. When interplaying with superconductivity, Josephson currents assisted by the helical edge state were studied theoretically [14–22] and experimentally [23–37]. A system supporting the helical band has the potential to generate an anomalous Josephson current [16,38]. In particular, a topological Josephson $\varphi_0$ junction was predicted in the presence of Zeeman field, where $\varphi_0$ was field-tunable phase shift in the current-phase relation [16]. However, the realization of such a junction is still a challenge [32] because, in the theoretical proposal, the orientation of the Zeeman field should match the spin alignment of the edge state, which is hard to acquire in real materials [6–9]. Moreover, the phase shift in two edge currents parallel to the junction may compensate for each other unless the device is finely constructed [16].

Recently, a flexible approach on manipulating the transport properties in materials was achieved by applying a high-frequency periodic driving field [39–42]. The transport properties were able to capture the signature of the topological phase transitions based on Floquet theory [43,44]. In three-dimensional (3D) systems, a Hall conductivity was induced when a nodal ring semimetal [45–49] or Dirac semimetal was periodically driven into a Floquet-Weyl semimetal [50,51]. Also, a spin filter effect [52] and anomalous Josephson current [53] were created when a Floquet-Weyl half semimetal phase occurred. In two-dimensional (2D) systems, a Floquet chiral edge state was predicted [54] and observed [55,56] in graphene. In addition, a quantum anomalous Hall insulator (QAHI) was expected in silicene [57], transition metal dichalcogenides [58], QSHIs [59,60], and the surface of 3DTIs [61], in which the driving field broke the time reversal symmetry. During the transition form QSHI phase to QAHI phase in a 2D Floquet TI, apart form the gap closing, an anisotropy was also induced in the helical edge states [59,60]. These anisotropic helical edge states can exist in a wide range of driving field amplitudes below the threshold value corresponding to the phase critical point. Being distinct from the isotropic ones, the velocities of the edge modes with opposite spin are of different magnitudes. Although such an anisotropy was first mentioned in an early work on silicene [57], it was nearly neglected in following works [51–53,59,60]. Moreover, the one-dimensional helical edge states can be investigated separately [62–66]. When interacting with the magnetic component of a circularly polarized electromagnetic wave, it was expected that the quantized photocurrent can be induced by the chiral anomaly in one of the edge states of a QSHI [65,66].

In this work, we find that when the supercurrent is mainly carried by the anisotropic edge states, the current-phase relations of a Josephson junction mediated by a light-dressed TI can be electrically modulated. The setup is depicted in Fig. 1(a). We suppose that the radiation is restricted within
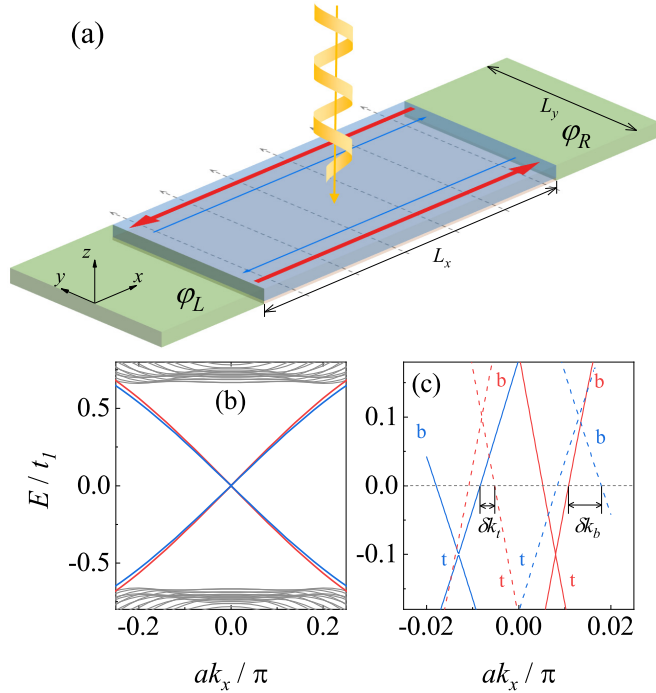
---

*phjfliu@gzhu.edu.cn
†wujs@sustech.edu.cn

FIG. 1. (a) Schematic of a Josephson junction composed of a topological insulator sandwiched by two conventional *s*-wave superconductors characterized by macroscopic phases $\varphi_{L/R}$. The length and width of the junction are $L_x$ and $L_y$, respectively. The central topological insulator is irradiated by a high-frequency periodic driving field, resulting in anisotropic helical edge states, where the spin-up (spin-down) edge modes with a higher (lower) velocity are labeled by thicker red (thinner blue) arrows. (b) The energy spectrum of a light-dressed topological insulator ribbon confined in the *y*-direction calculated form Eq. (16) without gate voltage and transverse electric field. (c) The electric and hole dispersions of anisotropic helical edge states. The spin-up (spin-down) electron/hole modes represented by the red (blue) solid/dashed lines and the top/bottom edge modes are labeled as t/b. the net momentum of the Cooper pair at two edge are labeled as $\delta k_{t,b}$. The parameters are $t_1 = 1, t_2 = 0.5t_1, M = 2t_1, L_y = 30$. The gate voltage $\mu_D$ and transverse electric potential $V$ is $\{\mu_D, V\} = \{0, 0\}$ in (b) and $\{\mu_D, V\} = \{0.1t_1, 0.2t_1\}$ in (c). The parameters of the driving field is $\eta = 1$ and we choose $\hbar\omega = 10t_1$ and $ak_A = 0.5$ to clarify the exhibition.

the central TI region, so that its influence on the superconducting leads can be neglected. The interaction between the periodically driving field and superconductors may induce odd-frequency superconducting pairs composed of electrons between different Floquet sidebands [67], which is beyond our discussions. We also assume that only the electrical component of the radiation is considered and the radiation is applied to the central region homogeneously, so that the photocurrent in one edge can be compensated by that in the other edge [64]. With these simplifications, we find that, due to the photoinduced anisotropy and spin-momentum locking nature in the edge channels, an effective Zeeman field that automatically matches the spin alignment of the edge states is induced by the electrical potential. As a result, a 0-$\pi$ phase transition [see Fig. 2(a)] in the current-phase relation is caused by the gate
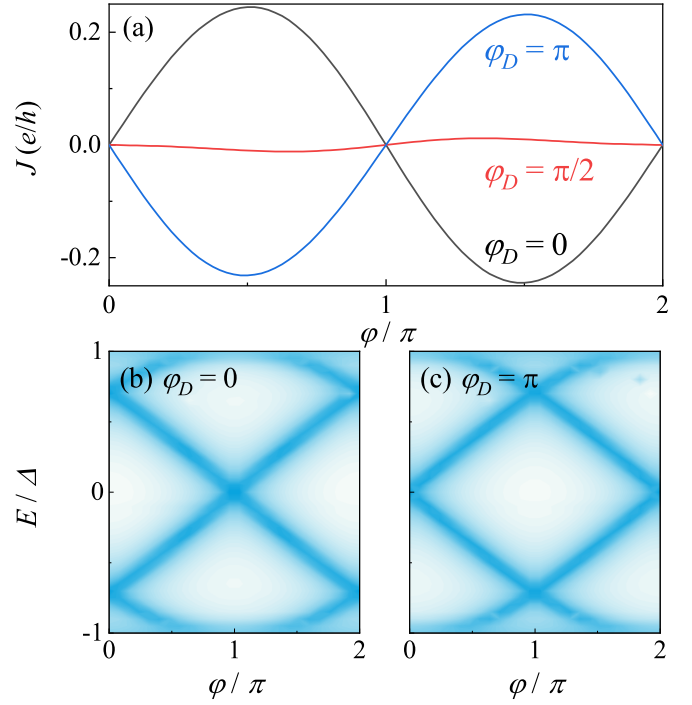


FIG. 2. (a) The current-phase relation with 0-$\pi$ phase transition and the Andreev bound states spectra corresponding to the (b) 0-phase and (c) $\pi$-phase current. The length of the junction is $L_x = 1998a$ and $\mu_D = 0.15t_1$ for $\varphi_D = \pi$. We choose $t_0 = t_1$, $\mu_{SC} = 2.2t_0$, $\Delta_0 = 0.005t_0$, and $T/T_c = 0.1$ in the superconductor leads and $t_c = t_0$. The parameter of the driving field is $\hbar\omega = 50t_1$, $ak_A = 0.5$. Other parameters are the same as those in Fig. 1(b).

voltage. In addition, without subtly constructing the junction, an arbitrary ground-state phase difference is obtained [see Fig. 3(a)], which is directly proportional to the product of the transverse electric field and the area of the junction. Additionally, we also find that through a joint manipulation of both the gate voltage and transverse electric field the supercurrent can become solely contributed to by one of the edges. Our work provides an alternative access to manipulate superconducting devices based on TIs.

The article is organized as followed. The Hamiltonian of light-dressed TIs as well as the anisotropic helical edge states are introduced in Sec. II. In Sec. III, the Josephson current assisted by the anisotropic helical edge states is qualitatively analyzed with some assumptions, which is further confirmed by the following numerical calculations and some results beyond the assumptions are discussed as well. The conclusion is given in Sec. IV.

## II. EDGE STATE OF LIGHT-DRESSED TOPOLOGICAL INSULATORS

In the basis of $|s, \uparrow\rangle$, $|p_x + ip_y, \uparrow\rangle$, $|s, \downarrow\rangle$, and $|-(p_x - ip_y), \downarrow\rangle$, the Hamiltonian of a TI written in a square lattice in the *x*-*y* plane is [7,8,59,68]

$$H(\boldsymbol{k}) = M_k\sigma_0\tau_z + 2t_2[\sin(ak_x)\sigma_z\tau_x - \sin(ak_y)\sigma_0\tau_y], \quad (1)$$

with the lattice constant $a = 1$, $\boldsymbol{k} = (k_x, k_y)$, and $M_k = M - 4t_1 + 2t_1[\cos(ak_x) + \cos(ak_y)]$, where $M$ and $t_{1,2}$ are model
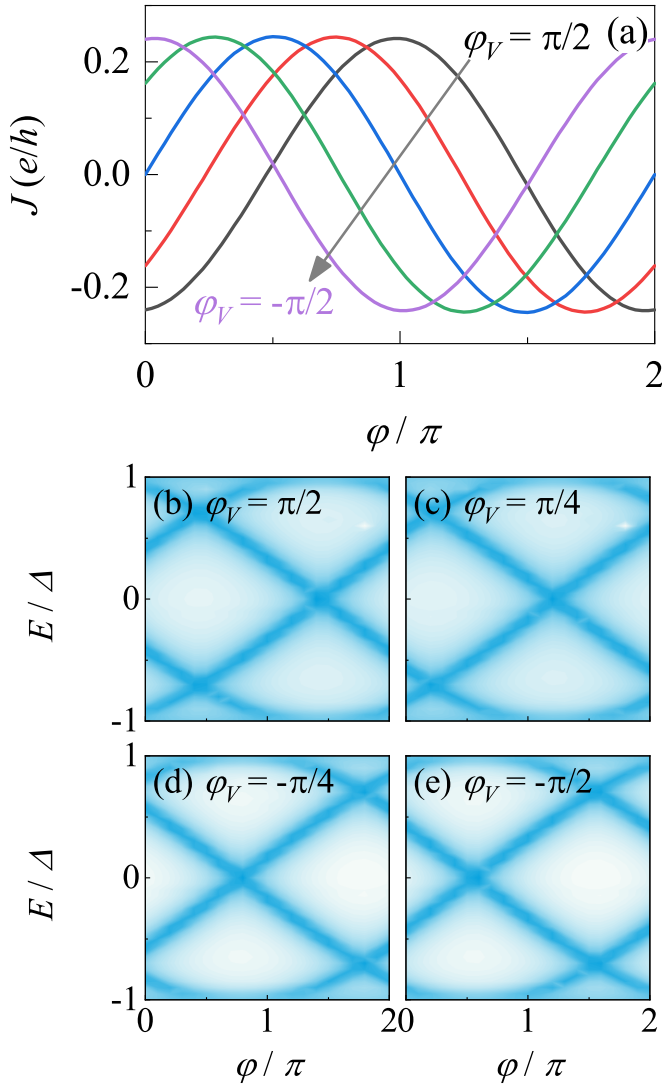
FIG. 3. (a) The current-phase relation with $\varphi_V$ varying from $\pi/2$ to $-\pi/2$ in the step of $\pi/4$, corresponding to Andreev bound states spectra exhibited in (b)–(e). The gate voltage is absent and $V = 0.15t_1$ for $\varphi_V = \pi$. Other parameters are the same as those in Fig. 2.

parameters and we choose $M$, $t_{1,2} > 0$ without loss of generality. $\sigma_0$ ($\tau_0$) and $\boldsymbol{\sigma}$ ($\boldsymbol{\tau}$) are the unit matrix and the Pauli matrices for the spin (orbital) degree of freedom, respectively. When the $z$ axis is the spin-quantization axis, the system supports spin-momentum locking isotropic helical edge states, in which spin-up (parallel to the $z$ axis) electrons propagate in one direction and the spin-down (antiparallel to the $z$ axis) ones propagate in the opposite direction, and both types of electrons travel in the same magnitude of velocity.

An out-of-plane electromagnetic wave [see Fig. 1(a)] can be written as a time-dependent vector potential [39]

$$\boldsymbol{A}(t) = \frac{E_0}{\omega}(\cos\omega t, \eta\sin\omega t), \quad (2)$$

where $E_0$ is the strength of the electric component of the wave with a frequency $\omega$ and $\eta = +1$ ($-1$) represents right (left)-handed circular polarization. Through the Peierls substitution, $\boldsymbol{k} \to \boldsymbol{k} + e\boldsymbol{A}(t)/\hbar$, a time-periodic Hamiltonian is

obtained $H(\boldsymbol{k}, t)$. Using Floquet theory, in the off-resonant regime where the energy of the incident photon $\hbar\omega$ is larger than the bandwidth of the system, an effective Hamiltonian takes the form as [43,44]

$$H_{eff}(\boldsymbol{k}) = H_0(\boldsymbol{k}) + \sum_{n>0}\frac{[H_{+n}(\boldsymbol{k}), H_{-n}(\boldsymbol{k})]}{n\omega} + \hat{O}\left(\frac{1}{\omega^2}\right), \quad (3)$$

where $H_n(\boldsymbol{k}) = \mathcal{T}^{-1}\int_{-\mathcal{T}/2}^{\mathcal{T}/2}dt H(\boldsymbol{k}, t)e^{-in\omega t}$ are the Fourier components of the $H(\boldsymbol{k}, t)$ with the period $\mathcal{T} = 2\pi/\omega$. After some algebra, the light-dressed Hamiltonian of a TI is

$$H_{eff}(\boldsymbol{k}) = H_0(\boldsymbol{k}) + H_l(\boldsymbol{k}), \quad (4)$$

with

$$H_0(\boldsymbol{k}) = M'_k\sigma_0\tau_z + 2J_0t_2[\sin(ak_x)\sigma_z\tau_x - \sin(ak_y)\sigma_0\tau_y], \quad (5)$$

and

$$H_l(\boldsymbol{k}) = \eta\lambda_1\sigma_z\tau_z + \eta\lambda_2[\sin(ak_x)\tau_x - \sin(ak_y)\sigma_z\tau_y], \quad (6)$$

where $M'_k = M - 4t_1 + 2J_0t_1[\cos(ak_x) + \cos(ak_y)]$, $\lambda_1 = 8(J_1t_2)^2/(\hbar\omega)$, $\lambda_2 = 8J_1^2t_2t_1/(\hbar\omega)$, and $J_n = J_n(ak_A)$ with $J_n(x)$ being the $n$th-order Bessel function. Here, a dimensionless parameter is introduced, $ak_A = aeE_0(\hbar\omega)^{-1}$, to renormalize the amplitude of driving, and we choose natural units with $\hbar = 1 = e$.

Without inducing significant deviations in our results, some of the higher-order terms such as $\cos(ak_{x,y})\sin(ak_{y,x})$ are replaced by $\sin(ak_{y,x})$ for simplifying the following numerical calculations. Moreover, in the process of obtaining Eq. (4) from Eq. (3), only $H_0$ and $H_{\pm 1}$ are involved, while the terms containing $J_{|n|\geqslant 2}(ak_A)$ are ignored because, in this work, we focus on the regime $ak_A < 1$ in which $J_n(ak_A)$ decreases rapidly with the increasing of $|n|$ [47,50,53].

Equation (6) describes two main photoinduced effects, which are (i) that the strengths of band inversion of each spin subband are, respectively, modified by $\lambda_1$ and (ii) that an anisotropy is caused in helical edge states through $\lambda_2$ [see Fig. 1(b)]. The first effect provides an alternative method to realize the QAHI, other than magnetic doping, which is explicitly demonstrated in some previous works [59,60]. However, in those works, the second effect was neglected because of its small magnitude and no phase transition concerned.

Now we focus on the anisotropic helical edge states. Consider a quantum confinement along the $y$ direction, deducing from Eq. (4), the low-energy Hamiltonian of the helical edge state is [69]

$$H_{edge}^s(k_x) = s(\eta v_t\sigma_0 + v\sigma_z)\hbar k_x, \quad (7)$$

where $\hbar v = 2J_0at_2$, $\hbar v_t = a\lambda_2$, $s = 1$, and $-1$ for the bottom ($y = -L_y/2$) and top ($y = +L_y/2$) edges. Equation (7) can be confirmed by the energy spectrum of a light-dressed TI ribbon depicted in Fig. 1(b). The dispersion of each edge mode is tilted because of $v_t$, which is similar to the tilted Weyl cone in Weyl semimetals [70,71]. In some previous works on type-I Weyl semimetals [72–74], it was demonstrated that, due to the tilting effect, an effective Zeeman field was induced by the electrical potential. This is also valid for a light-dressed TI. When adding an electrical potential $H_{edge}^s(k_x) - \mu\sigma_0$, an

effective Zeeman field $\eta v\mu/v_t\sigma_z$ is obtained after a substitution $k_x \rightarrow q_x = k_x - s\eta\mu/(\hbar v_t)$. Importantly, the direction of the effective Zeeman field automatically matches the spin alignment of the edge state, which is of great potential in manipulating the edge states of a TI.

Experimentally, it is a challenge to apply a Zeeman field exactly matching the spin alignment of the helical edge state, which tends to be affected by the imperfection of the crystalline structure and lacking symmetries in real materials. For example, in a HgTe/CdTe quantum well, the *preferential* spin-polarizing direction lies close to the plane of TI and perpendicular to the edges [7–9]. This indicates that the required Zeeman field will inevitably cause an out-of-plane component that may cause other unwanted side effects to the device, such as the quantized Landau levels and the Doppler shift [17,21]. Now, by virtue of the crossover of the spin-momentum locking nature and the photoinduced anisotropy, the effective Zeeman field automatically matches the spin alignment of the edge state, providing an alternative electrical approach to manipulate the edge state, which is of more flexibility and less ambiguity compared with an external magnetic field.

## III. ELECTRICALLY MODULATED TOPOLOGICAL JOSEPHSON JUNCTION

### A. Qualitative analysis

Inspired by previous works [16,17], we propose that the anisotropic edge states provide an accessible method to electrically modulate the current-phase relation of a Josephson junction mediated by a light-dressed TI. The junction depicted in Fig. 1(a) is composed of a light-dressed TI sandwiched by two conventional *s*-wave superconductors (SCs) characterized by macroscopic phases labeled as $\varphi_L$ and $\varphi_R$, respectively. The length and width of the junction are $L_x$ and $L_y$, respectively. Here, we first simply carry out a qualitative analysis on the current-phase relation, which is further confirmed by the numerical simulation demonstrated in Sec. III B.

If the width of the junction is sufficiently large and the Fermi level is within the bulk gap, the total Josephson current can be considered as the joint contributions from two individual edges. In the long junction limit and neglecting the higher harmonic terms, the current can be approximately written as [22,75]

$$J \approx J_b \sin(\varphi + \delta k_b L_x) + J_t \sin(\varphi + \delta k_t L_x), \quad (8)$$

where $J_{b/t}$ is the magnitude of the current flowing in the bottom/top edges, which depends on the details of the junction, $\varphi = \varphi_R - \varphi_L$ is the phase difference between two SC leads, and $\delta k_{b/t} L_x$ is an additional phase shift acquired in the TI region. Since in our proposal two edges have the same length, the net momentum of the Cooper pair $\delta k_{b/t}$ plays a crucial role in manipulating the current-phase relation [see Fig. 1(c)].

In the presence of gate voltage and the transverse electric field, anisotropic edge states in a light-dressed TI can be described by the one-dimensional (1D_ Bogoliubov–de Gennes (BdG) Hamiltonian

$$H_{\text{BdG}}^s(k_x) = s(\eta v_t\sigma_0 + v\sigma_z)\hbar k_x\xi_0 - (sV + \mu_D)\sigma_0\xi_z, \quad (9)$$

where $\xi_0$ and $\boldsymbol{\xi}$ are the unit matrix and the Pauli matrices in Nambu space, $V = eE_yL_y/2$ is half of the voltage difference between two edges, and $E_y$ is the strength of the transverse electric field. The corresponding dispersions are $E_{e,\uparrow(\downarrow)}^s(k_x) = s\eta v_t\hbar k_x + (-)sv\hbar k_x - (sV + \mu_D)$ for the electron bands and $E_{h,\uparrow(\downarrow)}^s = -E_{e,\uparrow(\downarrow)}^s(-k_x)$ for the hole bands. $\delta k_{b/t}$ can be found by solving equations $E_{e/h,\uparrow(\downarrow)}^s(k_x) = 0$ and the additional phase shifts are

$$\delta k_b L_x = (k_{e,\uparrow}^{-1} - k_{h,\downarrow}^{-1})L_x = -\varphi_D - \varphi_V, \quad (10)$$

and

$$\delta k_t L_x = (k_{e,\downarrow}^{+1} - k_{h,\uparrow}^{+1})L_x = +\varphi_D - \varphi_V, \quad (11)$$

where

$$\varphi_D = \eta\alpha\mu_D L_x, \quad (12)$$

and

$$\varphi_V = \eta\alpha V L_x = \eta\alpha eE_yS/2, \quad (13)$$

are the phase shift originating from the gate voltage and the transverse electric field, respectively, with $\hbar\alpha = 2v_t/(v^2 - v_t^2)$ and $S = L_yL_x$. Substituting Eqs. (10) and (11) into Eq. (8), the total supercurrent can be rewritten as

$$J \approx J_0 \cos\varphi_D \sin(\varphi - \varphi_V), \quad (14)$$

where we assumed that the current flowing in two edges are of the same magnitude, i.e., $J_t = J_b = J_0$. The main features of the Josephson current captured by Eq. (14) are as follows. (i) Due to the crossover of photoinduced anisotropy and the spin-momentum locking nature of the helical edge state, the sign of the supercurrent is reversed by the gate voltage as $\varphi_D = \pi$, resulting to a 0-$\pi$ phase transition in the junction [see Fig. 2(a)]. Similar results can be obtained by a Zeeman field along the spin quantization axis of the helical edges, indicating that an effective Zeeman effect is induced by the gate voltage in the anisotropic helical edge states. (ii) Without subtly constructing the junction, the current-phase relation is shifted by $\varphi_V$ [see Fig. 3(a)], which is directly proportional to the product of the transverse electric field and the area of the junction.

The effect of $v_t/v$ on phase shift is measurable for a large $L_x$, although it is negligible when studying photoinduced topological phase transitions [59,60]. The situation concerning QAHI is beyond our current consideration. One of the reasons is Andreev reflection is forbidden at the TI-SC interface because of the lack of a chiral edge state with opposite spin [53]. As a result, the Josephson current vanishes and may be recovered by the activation of spin-flipping at interfaces by two ferromagnets, which is similar to the situation of an anomalous Josephson current through a noncoplanar ferromagnetic trilayer [76,77].

### B. Numerical results and discussions

Now numerical results are provided to verify the qualitative analysis above, especially Eq. (14). The SC-TI-SC junction depicted in Fig. 1(a) can be described by the following Hamiltonian:

$$H_J = H_{TI} + \sum_{p=L,R}(H_p + T_p), \quad (15)$$

where

$$H_{TI} = \sum_{i,j} \hat{h}_0 C_{i,j}^\dagger C_{i,j} + \hat{h}_x C_{i+1,j}^\dagger C_{i,j} + \hat{h}_y C_{i,j+1}^\dagger C_{i,j} + \text{H.c.},$$
(16)

is the tight-binding version of the Hamiltonian in Eq. (4)

$$H_p = \sum_{i,j} [\hat{h}_{sc} C_{i,j}^\dagger C_{i,j} + \sum_\sigma \sigma \Delta e^{i\varphi_p} C_{i,j,\sigma} C_{i,j,\sigma}$$
$$- \hat{t}_{sc}(C_{i+1,j}^\dagger C_{i,j} + C_{i,j+1}^\dagger C_{i,j}) + \text{H.c.}], \quad (17)$$

is the Hamiltonian of the left ($p = L$) and right ($p = R$) SCs, and

$$T_p = \sum_{i=0/L_x,j} \hat{t}_c C_{i+1,j}^\dagger C_{i,j} + \text{H.c.},$$
(18)

couples the $p$-SCs to the TI. The components are

$$\hat{h}_0 = (M - 4t_1)\xi_z\sigma_0\tau_z + \eta\lambda_1\xi_z\sigma_z\tau_z + \hat{h}_E,$$
(19)

$$\hat{h}_x = J_0(t_1\xi_z\sigma_0\tau_z - it_2\xi_0\sigma_z\tau_x) - i\eta\lambda_2/2\xi_0\sigma_0\tau_x,$$
(20)

$$\hat{h}_y = J_0(t_1\xi_z\sigma_0\tau_z + it_2\xi_0\sigma_0\tau_y) + i\eta\lambda_2/2\xi_z\sigma_z\tau_y,$$
(21)

with

$$\hat{h}_E = -[\mu_D + V(1 - j/L_y)]\xi_z\sigma_0\tau_0$$

describing the effect of the gate voltage $\mu_D$ measured from zero energy and the transverse voltage $V = eE_y L_y/2$ in Eq. (16) and

$$\hat{h}_{sc} = (4t_0 - \mu_{SC})\xi_z\sigma_0\tau_0,$$
(22)

$$\hat{t}_{sc} = -t_0\xi_z\sigma_0\tau_0$$
(23)

in Eq. (17) with a chemical potential $\mu_{SC}$, macroscopic phases $\varphi_\alpha$. The finite-temperature order parameter is $\Delta = \Delta_0 \tanh(1.74\sqrt{T_c/T - 1})$ with the critical temperature $T_c$ and $\hat{t}_c = -t_c\xi_z\sigma_0\tau_0$ in Eq. (18). Here $C_{i,j} = \{c_{i,j}, c_{i,j}^\dagger\}^T$ with $c_{i,j} = \{c_{i,j,s,\uparrow}, c_{i,j,p,\uparrow}, c_{i,j,s,\downarrow}, c_{i,j,p,\downarrow}\}^T$ and $c_{i,j,s/p,\uparrow/\downarrow}$ ($c_{i,j,s/p,\uparrow/\downarrow}^\dagger$) is the annihilation (creation) operator of the $s/p$ orbit electron at site $\{i, j\}$ with spin $\uparrow/\downarrow$ and the notion $\sigma = \pm 1$ represents spin up and down. Without loss of generality, we choose $t_1 = 1$ as the energy unit, $M = 2t_1$ and $t_2 = 0.5t_1$ in TI. $t_0 = t_1$, $\mu_{SC} = 2.2t_0$, and $\Delta_0 = 0.005t_0 \ll \mu_{SC}$ in SCs. We choose $\hbar\omega = 50t_1$ to meet the high-frequency limit, which is sufficiently larger than the band gap ($\sim t_1$) and the bandwidth ($\sim 10t_1$) in the undressed TI. Only the right-handed circularly polarized driven ($\eta = +1$) is concerned here, while the case with $\eta = -1$ is simply obtained by $\varphi_{D/V} \rightarrow -\varphi_{D/V}$.

Using the lattice Green's function method, the Josephson current through column $l$ in the TI is [53,78]

$$J = \frac{1}{h} \int_{-\infty}^{\infty} \text{Tr}[\hat{h}_x^\dagger \hat{e} G_{l,l-1}^< - \hat{e}\hat{h}_x G_{l-1,l}^<]dE,$$
(24)

where $\hat{e} = -e\eta_z\sigma_0\tau_0$ is the charge matrix. In equilibrium, the lesser-than Green's function is calculated by $G^< = f(E)[G^a - G^r]$ where $f(E)$ is the Fermi-Dirac distribution function. The retarded Green's function is

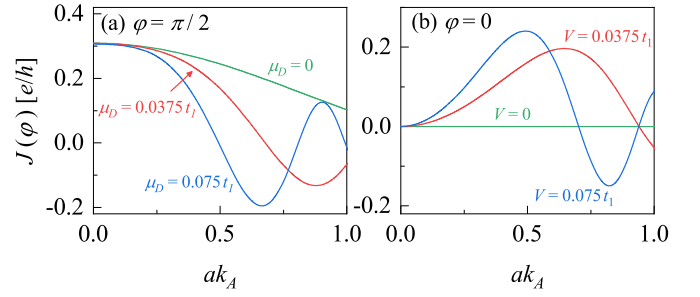$$G^r(E) = \frac{1}{E - H_{TI} - \Sigma_L^r(E) - \Sigma_R^r(E)},$$
(25)



FIG. 4. The Josephson current via $ak_A$ at a fixed phase difference (a) $\varphi = \pi/2$ and (b) $\varphi = 0$ in various $\mu_D$ and $V$, respectively. And we choose $V = 0$ ($\mu_D = 0$) in (a) [(b)]. Parameters are the same as those in Fig. 2.

and $G^a = [G^r(E)]^\dagger$, where the retarded self-energy $\Sigma_{L/R}^r(E)$ representing the coupling with left/right SC lead can be calculated numerically by the recursive method [79–81] . In addition, the energies of the Andreev bound state (ABS) levels can be located by searching the peaks of the particle density within the SC gap at column $l$ ($1 \leqslant l \leqslant L$)

$$\rho_l = -\frac{1}{\pi}\text{Im}[\text{Tr}G_{l,l}^r]$$
(26)

at a given phase difference $\varphi$.

The numerical results exhibited in Fig. 2(a) confirm the 0-$\pi$ transition in the current-phase relation when $V = 0$, which is consistent with the qualitative analysis Eq. (14) when $\varphi_D = 0$ and $\pi$. In the case with $\varphi_D = \pi/2$, the higher harmonic terms dominate in the current, which is beyond the assumption in Eq. (8). The 0-$\pi$ transition via $\varphi_D$ is also confirmed by the ABS levels depicted in Figs. 2(b) and 2(c). The anomalous Josephson current induced by the transverse electric field and the corresponding ABS levels are exhibited in Fig. 3. The Josephson current has an arbitrary and tunable ground-state phase difference $\varphi_V$, which is directly proportional to the product of the transverse electric field $E_y$ and the area of the central TI $S$. The numerical results in Fig. 3 are well consistent with our qualitative analysis in Eq. (14) for $\varphi_D = 0$.

Figure 4(a) exhibits an oscillating supercurrent at a fixed phase difference $\varphi = \pi/2$ via the dimensionless driven field amplitude $ak_A$, where the sign of the current does not reverse unless the gate voltage is sufficiently large. On the other hand, when the transverse electric field is applied, as depicted in Fig. 4(b), a finite current is generated without phase difference as the driven field amplitude increases, resulting in the anomalous Josephson current. In both cases above, the current vanishes for a high-field amplitude because of the phase transition form QSHI to QAHI with one of the spin channel in the helical edge state merges into the bulk state.

Another feature predicted in Eq. (14) is that the current oscillates cosinusoidally and sinusoidally with respect to the gate voltage $\mu_D$ and transverse electric potential $V$, respectively. These oscillating behaviors whose periods are determined by the driven field amplitude $ak_A$ are also well consistent with Eq. (14) as shown in Figs. 5(a) and 5(b) with $V = 0$ and $\mu_D = 0$, respectively. It should be noted that for a small $ak_A$, such as the blue curve with $ak_A = 0.2$, the
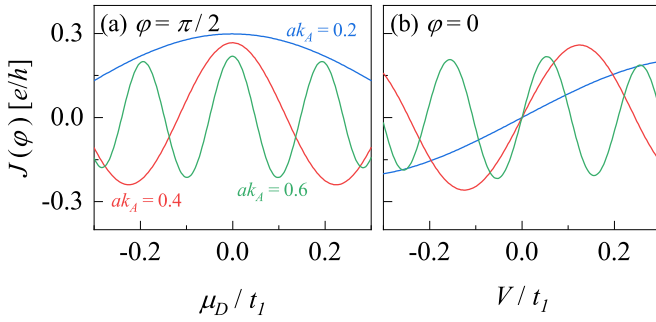
FIG. 5. The Josephson current via (a) $\mu_D$ with $\varphi = \pi/2$ and (b) $V$ with $\varphi = 0$ in various $ak_A$. The parameters are the same as those in Fig. 4.

anomalous phase shift in the current is turned on by $V$ while a relatively larger $\mu_D$ is required to realize the 0-$\pi$ transition.

However, these oscillating forms are broken down in some situations. First, as shown in Fig. 6(a), when $V = 0$, the current decreases as $\mu_D$ increases. Similar behavior is also obtained when $V$ increases as in Fig. 6(b). This results from the suppression of the Andreev reflection amplitude at the SC-TI interfaces [17]. We numerically calculate the Andreev reflection probability in a TI-SC junction, which is described by an Hamiltonian $H_{TI} + H_R$ with $\varphi_R = 0$. The transverse distribution of the Andreev reflection probability crossed the junction is displayed in Fig. 6(c), which exhibits that the Andreev reflection at two edges are of the same probability and gain an identical suppression for finite $\mu_D$ or $V$. The suppression of Andreev reflection leads to a reduction on the supercurrent. Additionally, the distribution of the Andreev reflection probability also validates our previous assumption on $J_t = J_b = J_0$ when deducing Eq. (14).
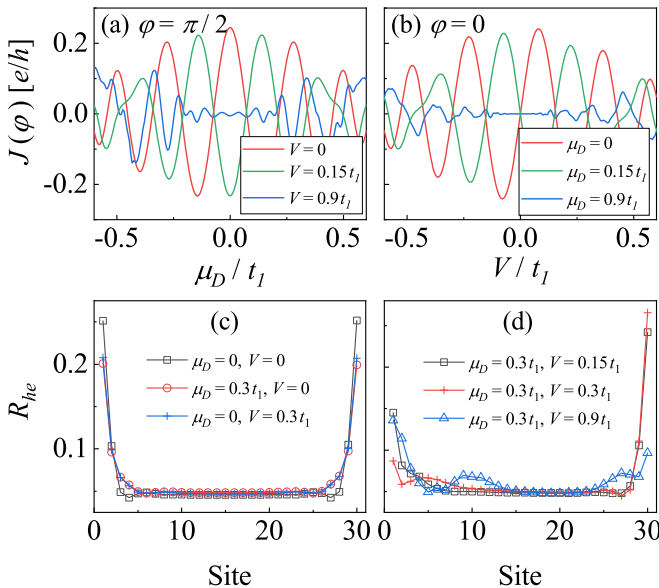


FIG. 6. The Josephson current via (a) $\mu_D$ with $\varphi = \pi/2$ and (b) $V$ with $\varphi = 0$. (c,d) The distribution of Andreev reflection probability $R_{he}$ at TI-SC interface in the direction perpendicular to the junction. The parameters are the same as those in Fig. 4.

In Fig. 6(a), the oscillating pattern further diverges from the perfect cosinusoidal form for a finite $V$. We argue that the reason for this is that the currents flowing in two edges become different from each other and the total current cannot be described by Eq. (14). This is the so-called asymmetric Josephson junction mediated by a TI without inversion symmetry [22], where the supercurrents along two edges are of different magnitudes. Although in this situation the accurate expression of the current is beyond our discussions, the inequality with two edge currents can be revealed in the distribution of the Andreev reflection probability depicted in Fig. 6(d). Compared with Fig. 6(c), it is obvious that the inversion symmetry is broken because of the coexistence of gate voltage and transverse electric field in the anisotropic edge states. Only the gate voltage or the transverse electric field alone cannot result from a broken inversion symmetry, which also is revealed in the ABS shown in Figs. 2 and 3. Moreover, it is worth noting that, when $|\mu_D| = |V|$, the Andreev reflection process in one edge is greatly suppressed and the total current is solely contributed to by the other edge. In addition, when the Fermi level crosses the bulk band because of the large gate voltage, the bulk contribution becomes dominant and the current gains a significant increase. This also accounts for the behavior of the oscillating current in Fig. 6(b).

Finally, we estimate the necessary driving field intensities and frequencies in realizing the Josephson junction in a HgTe quantum well with a thickness $\sim 7$ nm [6–8]. Typically, the energy unit in a TI is $t_1 = 20$ meV corresponding to the bulk gap in the order of meV [59,68]. To meet the off-resonant limit, the energy of the incident photon is $\hbar\omega = 50t_1 = 1$ eV and thus the frequency is $\omega \approx 1.57 \times 10^{15}$ s$^{-1}$. To observe the Josepshon effect at $ak_A = 0.5$, a driving intensity on the order of $10^9$ W/cm$^2$ is required. The estimated intensity and the required frequency could be within experimental reach in the near future [55,56].

## IV. CONCLUSION

In conclusion, due to the periodically driven anisotropy in the helical edge states of a TI, an effective Zeeman field is induced by the electrical potential. Importantly, the effective Zeeman field automatically matches the spin alignment of the edge states, which overcomes some challenges in realizing a topological Josephson $\varphi_0$ junction based on ordinary TIs. By virtue of the flexibility in tuning the electrical potential, the current-phase relation in the SC-TI-SC junction can be finely manipulated. The main features of the current phase relation are captured by Eq. (14), including the 0-$\pi$ phase transition caused by the gate voltage and anomalous phase shift that is directly proportional to the product of the transverse electric field and the area of the junction. Our findings may have potential applications on the helical supercurrent in topological superconducting devices.

[1] M. Z. Hasan and C. L. Kane, Colloquium: Topological Insulators, Rev. Mod. Phys. **82**, 3045 (2010).

[2] X.-L. Qi and S.-C. Zhang, Topological Insulators and Superconductors, Rev. Mod. Phys. **83**, 1057 (2011).

[3] C. L. Kane and E. J. Mele, Quantum Spin Hall Effect in Graphene, Phys. Rev. Lett. **95**, 226801 (2005).

[4] C. L. Kane and E. J. Mele, $Z_2$ Topological Order and the Quantum Spin Hall Effect, Phys. Rev. Lett. **95**, 146802 (2005).

[5] C. Wu, B. A. Bernevig, and S.-C. Zhang, Helical Liquid and the Edge of Quantum Spin Hall Systems, Phys. Rev. Lett. **96**, 106401 (2006).

[6] B. A. Bernevig, T. L. Hughes, and S.-C. Zhang, Quantum Spin Hall Effect and Topological Phase Transition in HgTe Quantum Wells, Science **314**, 1757 (2006).

[7] M. König, S. Wiedmann, C. Brüne, A. Roth, H. Buhmann, L. W. Molenkamp, X.-L. Qi, and S.-C. Zhang, Quantum Spin Hall Insulator State in HgTe Quantum Wells, Science **318**, 766 (2007).

[8] M. König, H. Buhmann, L. W. Molenkamp, T. L. Hughes, C.-X. Liu, X.-L. Qi, and S.-C. Zhang, The Quantum Spin Hall Effect: Theory and Experiment, J. Phys. Soc. Jpn. **77**, 031007 (2008).

[9] X.-L. Qi, T. L. Hughes, and S.-C. Zhang, Fractional Charge and Quantized Current in the Quantum Spin Hall State, Nat. Phys. **4**, 273 (2008).

[10] C. Liu, T. L. Hughes, X.-L. Qi, K. Wang, and S.-C. Zhang, Quantum Spin Hall Effect in Inverted Type-II Semiconductors, Phys. Rev. Lett. **100**, 236601 (2008).

[11] L. Du, I. Knez, G. Sullivan, and R.-R. Du, Robust Helical Edge Transport in Gated InAs/GaSb Bilayers, Phys. Rev. Lett. **114**, 096802 (2015).

[12] X. Qian, J. Liu, L. Fu, and J. Li, Quantum spin Hall effect in two-dimensional transition metal dichalcogenides, Science **346**, 1344 (2014).

[13] S. Wu, V. Fatemi, Q. D. Gibson, K. Watanabe, T. Taniguchi, R. J. Cava, and P. Jarillo-Herrero, Observation of the quantum spin Hall effect up to 100 kelvin in a monolayer crystal, Science **359**, 76 (2018).

[14] L. Fu and C. L. Kane, Josephson current and noise at a superconductor/quantum-spin-Hall-insulator/superconductor junction, Phys. Rev. B **79**, 161408(R) (2009).

[15] S.-P. Lee, K. Michaeli, J. Alicea, and A. Yacoby, Revealing Topological Superconductivity in Extended Quantum Spin Hall Josephson Junctions, Phys. Rev. Lett. **113**, 197001 (2014).

[16] F. Dolcini, M. Houzet, and J. S. Meyer, Topological Josephson $\phi_0$ junctions, Phys. Rev. B **92**, 035428 (2015).

[17] G. Tkachov, P. Burset, B. Trauzettel, and E. M. Hankiewicz, Quantum interference of edge supercurrents in a two-dimensional topological insulator, Phys. Rev. B **92**, 045408 (2015).

[18] G. Tkachov, Giant spin splitting and 0-$\pi$ Josephson transitions from the Edelstein effect in quantum spin Hall insulators, Phys. Rev. B **95**, 245407 (2017).

[19] L. Bours, B. Sothmann, M. Carrega, E. Strambini, E. M. Hankiewicz, L. W. Molenkamp, and F. Giazotto, Topological SQUIPT Based on Helical Edge States in Proximity to Superconductors, Phys. Rev. Appl. **10**, 014027 (2018).

[20] L. Bours, B. Sothmann, M. Carrega, E. Strambini, A. Braggio, E. M. Hankiewicz, L. W. Molenkamp, and F. Giazotto, Phase-Tunable Thermal Rectification in the Topological SQUIPT, Phys. Rev. Appl. **11**, 044073 (2019).

[21] G. Blasi, F. Taddei, L. Arrachea, M. Carrega, and A. Braggio, Nonlocal Thermoelectricity in a Superconductor-Topological-Insulator-Superconductor Junction in Contact with a Normal-Metal Probe: Evidence for Helical Edge States, Phys. Rev. Lett. **124**, 227701 (2020).

[22] C.-Z. Chen, J. J. He, M. N. Ali, G.-H. Lee, K. C. Fong, and K. T. Law, Asymmetric Josephson Effect in Inversion Symmetry Breaking Topological Materials, Phys. Rev. B **98**, 075430 (2018).

[23] J. B. Oostinga, L. Maier, P. Schüffelgen, D. Knott, C. Ames, C. Brüne, G. Tkachov, H. Buhmann, and L. W. Molenkamp, Josephson Supercurrent through the Topological Surface States of Strained Bulk HgTe, Phys. Rev. X **3**, 021007 (2013).

[24] S. Cho, B. Dellabetta, A. Yang, J. Schneeloch, Z. Xu, T. Valla, G. Gu, M. J. Gilbert, and N. Mason, Symmetry Protected Josephson Supercurrents in Three-Dimensional Topological Insulators, Nat. Commun. **4**, 1689 (2013).

[25] S. Hart, H. Ren, T. Wagner, P. Leubner, M. Mühlbauer, C. Brüne, H. Buhmann, L. W. Molenkamp, and A. Yacoby, Induced superconductivity in the quantum spin Hall edge, Nat. Phys. **10**, 638 (2014).

[26] L. Galletti, S. Charpentier, M. Iavarone, P. Lucignano, D. Massarotti, R. Arpaia, Y. Suzuki, K. Kadowaki, T. Bauch, A. Tagliacozzo, F. Tafuri, and F. Lombardi, Influence of Topological Edge States on the Properties of Al/Bi$_2$Se$_3$/Al Hybrid Josephson Devices, Phys. Rev. B **89**, 134512 (2014).

[27] C. Kurter, A. D. K. Finck, Y. S. Hor, and D. J. Van Harlingen, Evidence for an Anomalous Current-Phase Relation in Topological Insulator Josephson Junctions, Nat. Commun. **6**, 7130 (2015).

[28] V. S. Pribiag, A. J. A. Beukman, F. Qu, M. C. Cassidy, C. Charpentier, W. Wegscheider, and L. P. Kouwenhoven, Edge-mode superconductivity in a two-dimensional topological insulator, Nat. Nanotechnol. **10**, 593 (2015).

[29] J. Wiedenmann, E. Bocquillon, R. S. Deacon, S. Hartinger, O. Herrmann, T. M. Klapwijk, L. Maier, C. Ames, C. Brüne, C. Gould, A. Oiwa, K. Ishibashi, S. Tarucha, H. Buhmann, and L. W. Molenkamp, $4\pi$-periodic Josephson supercurrent in HgTe-based topological Josephson junctions, Nat. Commun. **7**, 10303 (2016).

[30] Y. Pang, J. Wang, Z. Lyu, G. Yang, J. Fan, G. Liu, Z. Ji, X. Jing, C. Yang, and L. Lu, Spatially Resolved Gap Closing in Single Josephson Junctions Constructed on Bi$_2$Se$_3$ Surface, Chinese Phys. B **25**, 117402 (2016).

[31] E. Bocquillon, R. S. Deacon, J. Wiedenmann, P. Leubner, T. M. Klapwijk, C. Brüne, K. Ishibashi, H. Buhmann, and L. W. Molenkamp, Gapless Andreev bound states in the quantum spin Hall insulator HgTe, Nat. Nanotechnol. **12**, 137 (2017).

[32] A. Murani, A. Kasumov, S. Sengupta, Y. A. Kasumov, V. T. Volkov, I. I. Khodos, F. Brisset, R. Delagrange, A. Chepelianskii, R. Deblock, H. Bouchiat, and S. Guéron, Ballistic Edge States in Bismuth Nanowires Revealed by SQUID Interferometry, Nat. Commun. **8**, 15941 (2017).

[33] A. Assouline, C. Feuillet-Palma, N. Bergeal, T. Zhang, A. Mottaghizadeh, A. Zimmers, E. Lhuillier, M. Eddrie, P. Atkinson, M. Aprili, and H. Aubin, Spin-Orbit Induced Phase-Shift in Bi$_2$Se$_3$ Josephson Junctions, Nat. Commun. **10**, 126 (2019).

[34] G. Kunakova, A. P. Surendran, D. Montemurro, M. Salvato, D. Golubev, J. Andzane, D. Erts, T. Bauch, and F. Lombardi, Topological Insulator Nanoribbon Josephson Junctions: Evidence for Size Effects in Transport Properties, J. Appl. Phys. **128**, 194304 (2020).

[35] B. De Ronde, C. Li, Y. Huang, and A. Brinkman, Induced Topological Superconductivity in a BiSbTeSe$_2$-Based Josephson Junction, Nanomaterials **10**, 794 (2020).

[36] V. S. Stolyarov, D. S. Yakovlev, S. N. Kozlov, O. V. Skryabina, D. S. Lvov, A. I. Gumarov, O. V. Emelyanova, P. S. Dzhumaev, I. V. Shchetinin, R. A. Hovhannisyan, S. V. Egorov, A. M. Kokotin, W. V. Pogosov, V. V. Ryazanov, M. Y. Kupriyanov, A. A. Golubov, and D. Roditchev, Josephson Current Mediated by Ballistic Topological States in Bi$_2$Te$_{2.3}$Se$_0$.7 Single Nanocrystals, Commun. Mater. **1**, 38 (2020).

[37] W. X. Wu, Y. Feng, Y. H. Bai, Y. Y. Jiang, Z. W. Gao, Y. Z. Li, J. L. Luan, H. A. Zhou, W. J. Jiang, X. Feng, J. S. Zhang, H. Zhang, K. He, X. C. Ma, Q. K. Xue, and Y. Y. Wang, Gate Tunable Supercurrent in Josephson Junctions Based on Bi$_2$Te$_3$ Topological Insulator Thin Films, Chinese Phys. Lett. **38**, 037402 (2021).

[38] K. N. Nesterov, M. Houzet, and J. S. Meyer, Anomalous Josephson effect in semiconducting nanowires as a signature of the topologically nontrivial phase, Phys. Rev. B **93**, 174502 (2016).

[39] T. Kitagawa, T. Oka, A. Brataas, L. Fu, and E. Demler, Transport properties of nonequilibrium systems under the application of light: Photoinduced quantum Hall insulators without Landau levels, Phys. Rev. B **84**, 235108 (2011).

[40] A. Eckardt, Colloquium: Atomic quantum gases in periodically driven optical lattices, Rev. Mod. Phys. **89**, 011004 (2017).

[41] T. Oka and S. Kitamura, Floquet Engineering of Quantum Materials, Annu. Rev. Condens. Matter Phys. **10**, 387 (2019).

[42] M. S. Rudner and N. H. Lindner, Band structure engineering and non-equilibrium dynamics in Floquet topological insulators, Nat. Rev. Phys. **2**, 229 (2020).

[43] A. Eckardt and E. Anisimovas, High-Frequency Approximation for Periodically Driven Quantum Systems from a Floquet-Space Perspective, New J. Phys. **17**, 093039 (2015).

[44] M. Vogl, M. Rodriguez-Vega, and G. A. Fiete, Effective Floquet Hamiltonian in the Low-Frequency Regime, Phys. Rev. B **101**, 024303 (2020).

[45] C.-K. Chan, Y.-T. Oh, J. H. Han, and P. A. Lee, Type-II Weyl cone transitions in driven semimetals, Phys. Rev. B **94**, 121106(R) (2016).

[46] A. Narayan, Tunable point nodes from line-node semimetals via application of light, Phys. Rev. B **94**, 041409(R) (2016).

[47] Z. Yan and Z. Wang, Tunable Weyl Points in Periodically Driven Nodal Line Semimetals, Phys. Rev. Lett. **117**, 087402 (2016).

[48] K. Taguchi, D.-H. Xu, A. Yamakage, and K. T. Law, Photovoltaic anomalous Hall effect in line-node semimetals, Phys. Rev. B **94**, 155206 (2016).

[49] L. Li, H. H. Yap, M. A. N. Araújo, and J. Gong, Engineering topological phases with a three-dimensional nodal-loop semimetal, Phys. Rev. B **96**, 235424 (2017).

[50] R. Wang, B. Wang, R. Shen, L. Sheng, D. Y. Xing, Floquet Weyl semimetal induced by off-resonant light, Europhys. Lett. **105**, 17004 (2014).

[51] P.-H. Fu, H.-J. Duan, R.-Q. Wang, and H. Chen, Phase transitions in Three-Dimensional Dirac Semimetal Induced by off-Resonant Circularly Polarized Light, Phys. Lett. A **381**, 3499 (2017).

[52] X. S. Li, C. Wang, M. X. Deng, H. J. Duan, P. H. Fu, R. Q. Wang, L. Sheng, and D. Y. Xing, Photon-Induced Weyl Half-Metal Phase and Spin Filter Effect from Topological Dirac Semimetals, Phys. Rev. Lett. **123**, 206601 (2019).

[53] P.-H. Fu, J. Wang, J.-F. Liu, and R.-Q. Wang, Josephson Signatures of Weyl Node Creation and Annihilation in Irradiated Dirac Semimetals, Phys. Rev. B **100**, 115414 (2019).

[54] T. Oka and H. Aoki, Photovoltaic Hall effect in graphene, Phys. Rev. B **79**, 081406(R) (2009), **79**, 169901(E) (2009).

[55] Y. Chen, Y. Wang, M. Claassen, B. Moritz, and T. P. Devereaux, Observing Photo-Induced Chiral Edge States of Graphene Nanoribbons in Pump-Probe Spectroscopies, npj Quantum Mater. **5**, 84 (2020).

[56] J. W. McIver, B. Schulte, F. U. Stein, T. Matsuyama, G. Jotzu, G. Meier, and A. Cavalleri, Light-Induced Anomalous Hall Effect in Graphene, Nat. Phys. **16**, 38 (2020).

[57] M. Ezawa, Photoinduced Topological Phase Transition and a Single Dirac-Cone State in Silicene, Phys. Rev. Lett. **110**, 026603 (2013).

[58] P. X. Nguyen and W. K. Tse, Photoinduced Anomalous Hall Effect in Two-Dimensional Transition Metal Dichalcogenides, Phys. Rev. B **103**, 125420 (2021).

[59] M. N. Chen, W. Su, M. X. Deng, J. Ruan, W. Luo, D. X. Shao, L. Sheng, and D. Y. Xing, Photoinduced Topological Phase Transition and Spin Polarization in a Two-Dimensional Topological Insulator, Phys. Rev. B **94**, 205429 (2016).

[60] S. S. Dabiri, H. Cheraghchi, and A. Sadeghi, Light-Induced Topological Phases in Thin Films of Magnetically Doped Topological Insulators, Phys. Rev. B **103**, 205130 (2021).

[61] H. Xu, J. Zhou, and J. Li, Light-Induced Quantum Anomalous Hall Effect on the 2D Surfaces of 3D Topological Insulators, Adv. Sci. **8**, 2101508 (2021).

[62] B. Dóra, J. Cayssol, F. Simon, and R. Moessner, Optically Engineering the Topological Properties of a Spin Hall Insulator, Phys. Rev. Lett. **108**, 056602 (2012).

[63] S. Vajna, B. Horovitz, B. Dóra, and G. Zaránd, Floquet Topological Phases Coupled to Environments and the Induced Photocurrent, Phys. Rev. B **94**, 115145 (2016).

[64] J. Atteia and J. Cayssol, Photocurrent and Photoconductance of a Helical Edge State, Phys. Rev. B **100**, 245412 (2019).

[65] C. Fleckenstein, N. Traverso Ziani, and B. Trauzettel, Chiral Anomaly in Real Space from Stable Fractional Charges at the

Edge of a Quantum Spin Hall Insulator, Phys. Rev. B **94**, 241406(R) (2016).

[66] F. Dolcini, R. C. Iotti, A. Montorsi, and F. Rossi, Photoexcitation of Electron Wave Packets in Quantum Spin Hall Edge States: Effects of Chiral Anomaly from a Localized Electric Pulse, Phys. Rev. B **94**, 165412 (2016).

[67] J. Cayao, C. Triola, and A. M. Black-Schaffer, Floquet Engineering Bulk Odd-Frequency Superconducting Pairs, Phys. Rev. B **103**, 104505 (2021).

[68] J. Song, H. Liu, J. Liu, Y.-X. Li, R. Joynt, Q. Sun, and X. C. Xie, Quantum Interference in Topological Insulator Josephson Junctions, Phys. Rev. B **93**, 195302 (2016).

[69] S. Q. Shen, *Topological Insulators* (Springer-Verlag, Berlin, 2012).

[70] A. A. Soluyanov, D. Gresch, Z. Wang, Q. S. Wu, M. Troyer, X. Dai, and B. A. Bernevig, Type-II Weyl semimetals, Nature (London) **527**, 495 (2015).

[71] P. Li, Y. Wen, X. He, Q. Zhang, C. Xia, Z.-M. Yu, S. A. Yang, Z. Zhu, H. N. Alshareef, and X.-X. Zhang, Evidence for topological type-II Weyl semimetal $WTe_2$, Nat. Commun. **8**, 2150 (2017).

[72] C. Yesilyurt, Z. Bin Siu, S. G. Tan, G. Liang, and M. B. A. Jalil, Conductance Modulation in Weyl Semimetals with Tilted Energy Dispersion without a Band Gap, J. Appl. Phys. **121**, 244303 (2017).

[73] C. Yesilyurt, Z. Bin Siu, S. G. Tan, G. Liang, S. A. Yang, and M. B. A. A. Jalil, Anomalous Tunneling Characteristic of Weyl Semimetals with Tilted Energy Dispersion, Appl. Phys. Lett. **111**, 063101 (2017).

[74] C. Yesilyurt, Z. Bin Siu, S. G. Tan, G. Liang, S. A. Yang, and M. B. A. Jalil, Electrically Tunable Valley Polarization in Weyl Semimetals with Tilted Energy Dispersion, Sci. Rep. **9**, 4480 (2019).

[75] Y. Asano, Y. Tanaka, M. Sigrist, and S. Kashiwaya, Josephson Current in s -Wave-Superconductor/$Sr_2RuO_4$ Junctions, Phys. Rev. B **67**, 184505 (2003).

[76] J.-F. Liu and K. S. Chan, Anomalous Josephson current through a ferromagnetic trilayer junction, Phys. Rev. B **82**, 184533 (2010).

[77] J.-F. Liu and K. S. Chan, Relation between symmetry breaking and the anomalous Josephson effect, Phys. Rev. B **82**, 125305 (2010).

[78] Y. Xu, S. Uddin, J. Wang, Z. Ma, and J.-F. Liu, Electrically Modulated SQUID with a Single Josephson Junction Coupled by a Time Reversal Breaking Weyl Semimetal Thin Film, Phys. Rev. B **97**, 035427 (2018).

[79] S. Datta, *Electronic Transport in Mesoscopic Systems* (Cambridge University Press, Cambridge, England, 1997).

[80] M. P. L. Sancho, J. M. L. Sancho, and J. Rubio, Highly convergent schemes for the calculation of bulk and surface Green functions, J. Phys. F **15**, 851 (1985).

[81] D. S. Fisher and P. A. Lee, Relation between conductivity and transmission matrix, Phys. Rev. B **23**, 6851 (1981).